Int. J. Electrochem. Sci., 8 **(2013)** 4700 - 4711

International Journal of
ELECTROCHEMICAL
SCIENCE
www.electrochemsci.org

Effect of Electro-Oxidation Current Density on Performance of Graphite Felt Electrode for Vanadium Redox Flow Battery

Jingyu Xi[1,*], *Wenguang Zhang*[1,2], *Zhaohua Li*[1,2], *Haipeng Zhou*[1,2], *Le Liu*[1], *Zenghua Wu*[1], *Xinping Qiu*[1,2,*]

[1] Lab of Advanced Power Sources, Graduate School at Shenzhen, Tsinghua University, Shenzhen 518055, China.
[2] Key Lab of Organic Optoelectronics and Molecular Engineering, Department of Chemistry, Tsinghua University, Beijing 100084, China
(J. Xi and W. Zhang contributed equally to this work.)
[*]E-mail: qiuxp@tsinghua.edu.cn, xijingyu@gmail.com

Received: 25 January 2013 / *Accepted:* 28 February 2013 / *Published:* 1 April 2013

Electro-oxidation method is used to improve the electrolyte accessibility and reaction activity of the graphite felt (GF) electrode for vanadium redox flow battery (VRB). The effect of electro-oxidation current density on activity of oxidized graphite felt (OGF) is investigated and the optimized parameter is suggested. Scanning electron microscope result indicates that the surface of GF is etched and becomes rougher by electro-oxidation treatment. Cyclic voltammetry and electrochemical impedance spectroscopy results show that the OGF obtained at 50 mA/cm^2 (OGF-50) has the highest oxidation peak current density and lowest charge transfer resistance towards VO^{2+}/VO_2^+ redox reaction, due to the introduction of surface oxygen-containing active functional groups, which is further verified by X-ray photoelectron spectroscopy. VRB single cell using OGF-50 electrode also exhibits the best cell performance, with a voltage and energy efficiency of 87% and 77% at 60 mA/cm^2, respectively. Electro-oxidation method is environmentally friendly and controllable comparing with the tradition activation methods, such as concentrated acid treatment and high-temperature thermal treatment.

Keywords: Vanadium redox flow battery, Graphite felt, Electrode, Electro-oxidation

1. INTRODUCTION

Develop large-scale, high-efficient and long-life energy storage technology is very important for ensuring the grid security and promotes the use of renewable energy [1,2]. Among all kinds of physical and chemical energy storage technologies, vanadium redox flow battery (VRB) has become the fastest growing and most promising energy storage system due to its unique advantages such as

easily implementing large-scale, long cycle life, flexible design, fast response time, and deep-discharge capability [1-5]. VRB can be used in electricity storage for solar and wind power generation system, peak shaving for grid, distributed power supply, emergency power supply, and other fields [3-5].

Quite a few VRB demonstration prototypes with different power level have been established worldwide [3-5]. However, the drawbacks, such as low energy (power) density and fast capacity fading rate, still restrict the widely use of VRB. Vanadium electrolyte, ion-exchange membrane, and carbon-based felt electrode are three key materials of VRB, which determine the performance of the battery. Recently, significant progresses have been achieved in terms of high concentration vanadium electrolyte [6-8] and low vanadium ion permeability membrane [9-11] for VRB. The most commonly used electrode material for VRB is carbon fabric, e.g. graphite felt (GF), due to its self-standing structure, high electronic conductivity porous network and well chemical stability [3,4]. However, poor electrochemical activity and serious side reactions, for example hydrogen evolution in negative half-cell or oxygen evolution in positive half-cell, were found when pristine GF was used in VRB [4]. A variety of modification methods, including thermal activation [12], acid treatment [13], chemical-oxidation (Fenton's reagent treatment) [14], and electro-deposition of metals [15,16] have been investigated to improve the activity of the GF. Electro-oxidation is an environmental friendly and controllable technique for surface treatment of carbon based materials, which can introduce numerous types of oxygen-containing surface functional groups and increase the surface roughness [17]. Nonetheless, electro-oxidation of GF electrode for VRB has been rarely reported [18].

In previous work [19], we have pointed out that electro-oxidation method is a promising technology for the activity of GF electrode. Oxidized graphite felt (OGF) electrode with the oxidation degree of 560 mAh/g showed the best performance in cyclic voltammetry and VRB single cell test. In present work, the effect of current density on the surface morphology, oxygen-containing surface functional groups and electrochemical properties of OGF during the electro-oxidation process were studied in detail. These results are helpful to understand the electro-oxidation mechanism of GF and may provide optimized parameters for high-performance OGF electrode.

2. EXPERIMENTAL

2.1 Materials and electrode preparation

All the reagents used in this study are of analytical grade or otherwise specified. Polyacrylonitrile (PAN) based GF with thickness of 5 mm was purchased from Gansu Haoshi Carbon Fiber Co. Ltd. $VOSO_4 \cdot 4H_2O$ (>99%) was purchased from Shenyang Haizhongtian Fine Chemical factory and concentrated H_2SO_4 (98% wt) was obtained from Guangzhou Donghong Chemical Factory.

Pristine GF was cut into small pieces (1.5 cm × 1.5 cm), repeatedly washed with distilled water and dried at 70 ^oC for 48 h. Electro-oxidation was carried out in 1 M H_2SO_4 solution using GF plate as anode and graphite plate as cathode. The GF working electrode was prepared by pressing a piece of GF between two PVC sheets, one of the PVC sheet having a hole of 1.0 cm × 1.0 cm. The GF can be

connected with H_2SO_4 electrolyte through the hole. Another side of the GF was connected with a polished Ti plate current collector. The oxidation degree was kept at 560 mAh/g with the current density ranging from 10 to 200 mA/cm^2. The resulted OGF was seperated, washed thoroughly with distilled water, and then dried at 70 ^{o}C for 48 h. The electro-oxidation GF sample was denoted as OGF-x, in which x means the applied electro-oxidation current density.

To perform the VRB single cell test, the OGF samples with size of 5 cm × 5 cm were also prepared by the same electro-oxidation process.

2.2 Characterizations of the electrode

The surface morphology was characterized by scanning electron microscopy (SEM) on a Hitachi S-4800 instrument in which EDS analysis was used to analyze the surface element distribution. X-ray photoelectron spectroscopy (XPS) characterization was carried out on PHI5300 XPS instrument and the spectra were analyzed using Spectrum software (XPS PEAK 41).

Electrochemical measurements were carried out in a three-electrode cell using a Princeton Applied Research PARSTAT 2273 workstation at 25 ºC. A saturated calomel electrode (SCE) and graphite plate were used as reference and counter electrodes, respectively. All electrode potentials in this paper were referred to the SCE. Cyclic voltammetry (CV) was carried out in 0.015 M $VOSO_4$ + 3 M H_2SO_4 between 0.4 V and 1.4 V with a scan rate of 1 mV/s. Electrochemical impedance spectroscopy (EIS) was performed under open circuit potential (OCP) in 1.5 M $VOSO_4$ + 3 M H_2SO_4 with an excitation signal of 5 mV in the frequency range of 100 kHz to 10 mHz.

2.3 VRB single cell test

The VRB single cell used in charge-discharge test was fabricated by sandwiching the Nafion 117 membrane (6 cm × 6 cm) between two pieces of graphite felt electrodes (5 cm × 5 cm) and then clamping the sandwich between two graphite polar plates. At the beginning of charge-discharge test, 60 mL of 2 M VO^{2+} in 3 M H_2SO_4 solution was pumped into the positive side and 60 mL of 2 M V^{3+} in 3 M H_2SO_4 solution was pumped into the negative side. The charge-discharge test was carried out in the voltage range of 0.8-1.65 V using a NEWARE battery test system (BTS-6V3A) with a constant current density of 40-80 mA/cm^2.

3. RESULTS AND DISCUSSIONS

3.1 Characterizations of pristine GF

Morphology and electrochemical performances of pristine GF were studied by SEM, contact angle test, CV, and EIS method. Fig. 1 (a) shows the typical morphology of the GF, a 3D porous network derived from the fabric of smooth and clean graphite fibers with an average diameter of 15 μm. Fig. 1 (b) shows the contact angle (131 ^{o}) of water droplet on the surface of GF, indicating that the

surface energy of GF is very low and the wettability is very poor, which may result in the bad electrolyte accessibility during the VRB running process.

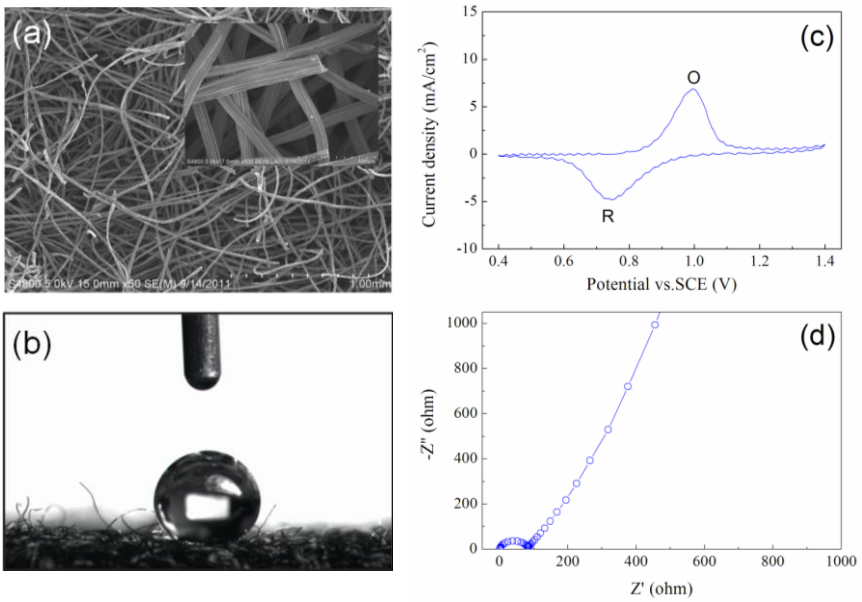

Figure 1. (a) Low magnification SEM image of pristine GF, inset shows an enlarged picture, (b) Contact angle image of water droplet on the surface of GF, (c) CV curve of VO^{2+}/VO_2^+ redox couple at GF in 0.015 M $VOSO_4$ + 3 M H_2SO_4 solution with a scan rate of 1mV/s, (d) Nyquist plot of GF in 1.5 M $VOSO_4$ + 3 M H_2SO_4.

Fig.1 (c) gives the CV curve of pristine GF in 0.015 M $VOSO_4$ + 3 M H_2SO_4 solution with a scan rate of 1mV/s. The anodic peak O and reduction peak R can be attributed to VO^{2+}/VO_2^+ redox reaction. The oxidation peak current density and the peak potential separation (ΔE_p) are 6.7 mA/cm^2 and 252 mV, respectively. Fig.1 (d) displays the Nyquist plot of pristine GF in 1.5 M $VOSO_4$ + 3 M H_2SO_4 solution, including a semicircle part at high frequency and a linear part at low frequency This suggests that the electrochemical process is mix-controlled by charge transfer and diffusion steps. The high frequency semi-arc arises from the charge transfer reaction at the electrolyte/electrode interface. while the radius of the semi-arc reflects the charge transfer resistance, R_{ct}. The low frequency linear part can be attributed to the diffusion processes associated with the diffusion of VO^{2+}/VO_2^+ in the 3D network of the electrode [19-22]. From Fig. 1 (c) and (d), it is clear that pristine GF exhibits poor electrochemical activity towards VO^{2+}/VO_2^+ redox reaction, which is consistent with the morphology results of GF shown in Fig. 1 (a) and (b).

3.2 Effect of electro-oxidation current density on the performance of OGF

In previous work, we have proved that electro-oxidation treatment can obviously improve the activity of GF and the oxidized graphite felt (OGF) electrode with the oxidation degree of 560 mAh/g exhibits the best performance in cyclic voltammetry and VRB single cell test [19]. In order to

understand the electro-oxidation mechanism of GF and to provide optimal parameters for high-performance OGF, the effect of electro-oxidation current density during electro-oxidation process on the surface morphologies, oxygen-containing surface functional groups and electrochemical properties of OGF were further studied. The oxidation degree was controlled at 560 mAh/g while the applied current density ranges from 10 to 200 mA/cm^2.

Fig. 2 compares the CV curves of VO^{2+}/VO_2^+ redox couple at OGF. The anodic peak O is associated with the oxidation of VO^{2+} to VO_2^+ and the corresponding reduction peak R appears at 0.9 V and 0.8 V, respectively. It is seen that the electro-oxidation current density has small effect on both the reduction peak potential and the reduction peak current density for all OGF samples. On the contrary, the oxidation peak current density and oxidation peak potential of OGF significantly change with the electro-oxidation current density. In addition, ΔE_p of all OGF (110-140 mV) are smaller than that of GF (252 mV), suggesting that the reversibility of the VO^{2+}/VO_2^+ redox reaction is improved after electro-oxidation.

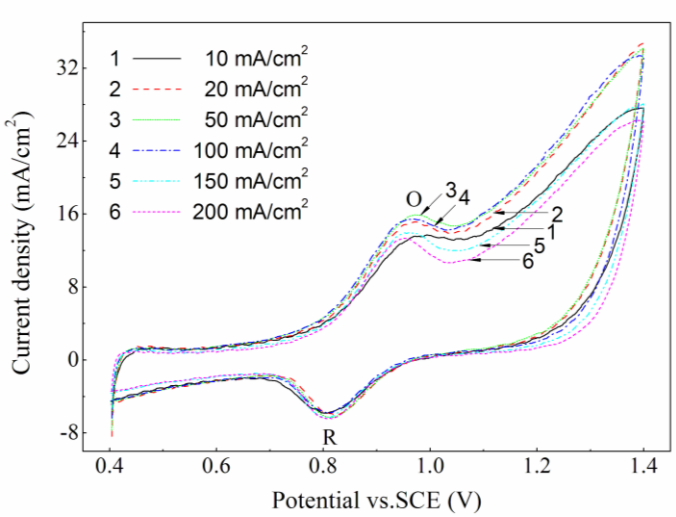

Figure 2. CV curves of VO^{2+}/VO_2^+ redox couple at OGF in 0.015 M $VOSO_4$ + 3 M H_2SO_4 solution with a scan rate of 1mV/s.

Fig. 3 shows the effect of electro-oxidation current density on the oxidation peak current density of VO^{2+}/VO_2^+ redox couple at OGF. All OGF samples display oxidation peak current density at least two times that of the pristine GF. This indicates that the electrochemical activity of OGF is enhanced significantly for VO^{2+}/VO_2^+ couple, which can be attributed to the formation of oxygen-containing groups on the surface of OGF. The oxygen-containing surface functional groups can provide active sites for VO^{2+}/VO_2^+ redox reaction [19]. As can be seen from Fig. 3, the oxidation peak current density of VO^{2+} to VO_2^+ first increases with the electro-oxidation current density from 10 to 50 mA/cm^2 and then decreases when electro-oxidation current density ranges from 100 to 200 mA/cm^2. This result suggests that electro-oxidation current density has significant effect on the electrochemical activity of OGF and only a moderate electro-oxidation process can provide the high-performance OGF. This phenomenon may be attributed to the fact that forming mechanism of active oxygen atoms

(O•) is changing with oxidation current density. When the electro-oxidation current density is too large or too low, the concentration of oxygen-containing functional groups (C-OH, COOH) on OGF surface can't provide enough active sites for the oxidation reaction of VO^{2+} to VO_2^+. From Fig. 3, it may be assumed that the concentration of C-OH and COOH functional groups acts as active sites and reaches an optimal value at the electro-oxidation condition of 50 mA/cm^2.

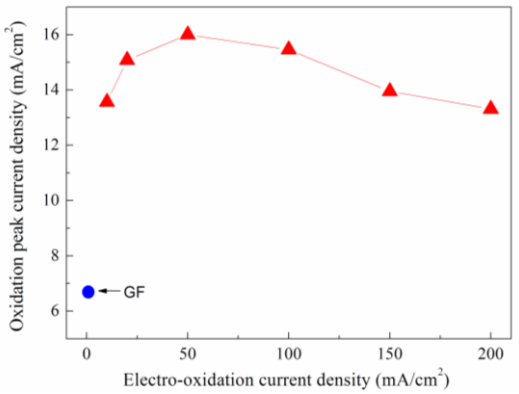

Figure 3. Effect of electro-oxidation current density on the oxidation peak current density of VO^{2+}/VO_2^+ redox couple at OGF.

EIS measurements were carried out to further investigate the electrode structure and charge transfer properties of OGF electrode obtained at various electro-oxidation current density. Fig. 4 (a) displays the Nyquist plots of OGF electrode in 1.5 M $VOSO_4$ + 3 M H_2SO_4 solution.

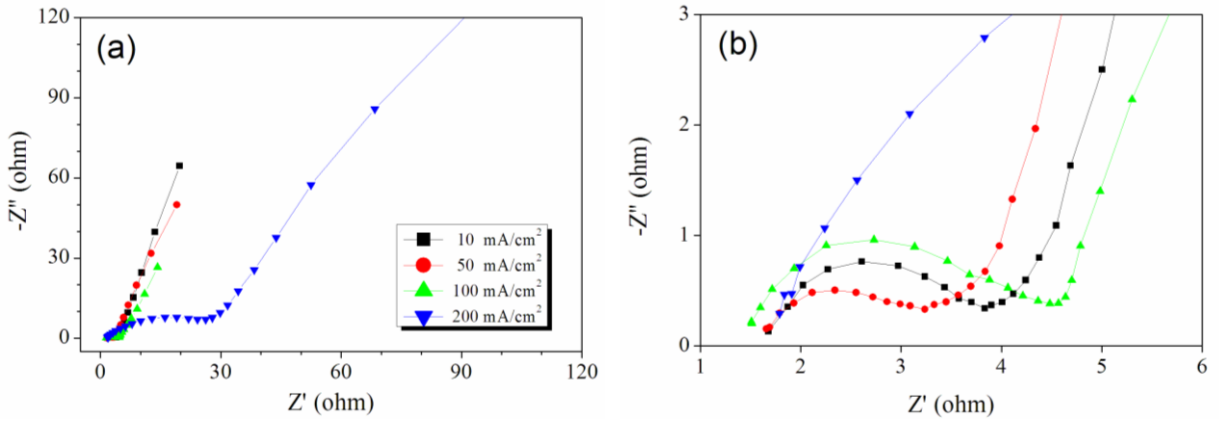

Figure 4. (a) Nyquist plot of OGF in 1.5 M $VOSO_4$ + 3 M H_2SO_4, (b) Enlarged high frequency part of figure (a).

All the Nyquist plots include a semicircle part at high frequency and a linear part at low frequency, suggesting that the electrochemical process was mix-controlled by charge transfer and diffusion steps, like the case of pristine GF shown in Fig.1 (d). In order to compare the R_{ct} of

VO^{2+}/VO_2^+ reaction on different OGF, the high frequency part of Fig. 4 (a) is enlarged and shown in Fig. 4 (b). It can be seen from Fig. 1 (d) and Fig. 4 (b) that the pristine GF electrode has the largest semi-arc radius, indicating that GF has the largest R_{ct} for VO^{2+}/VO_2^+. The magnitude of high frequency semi-arc of OGF decreases significantly with the electro-oxidation current density increasing from 0 to 50 mA/cm^2 and then increases with the electro-oxidation current density further increasing. The change tendency of R_{ct} is in agreement with the CV results shown in Fig. 3.

The improvement in the activity of OGF for VO^{2+}/VO_2^+ should be related to the novel surface state of OGF [19]. XPS measurements can provide direct information of surface functional groups and Fig.5 shows the XPS spectra of C 1s for OGF obtained at different electro-oxidation current density. The main peak at 284.7 eV can be attributed to graphitized carbon, and the other four peaks can be attributed to defects on the GF structure (285.1 eV), C-OH (286.3 eV), -COO & -C=O (286.8 eV), and COOH (288.9 eV) [17,19,20]. The contents of various surface groups of the OGF can be calculated based on Fig. 5 by measuring the relative peak areas and the results are listed in Table 1.

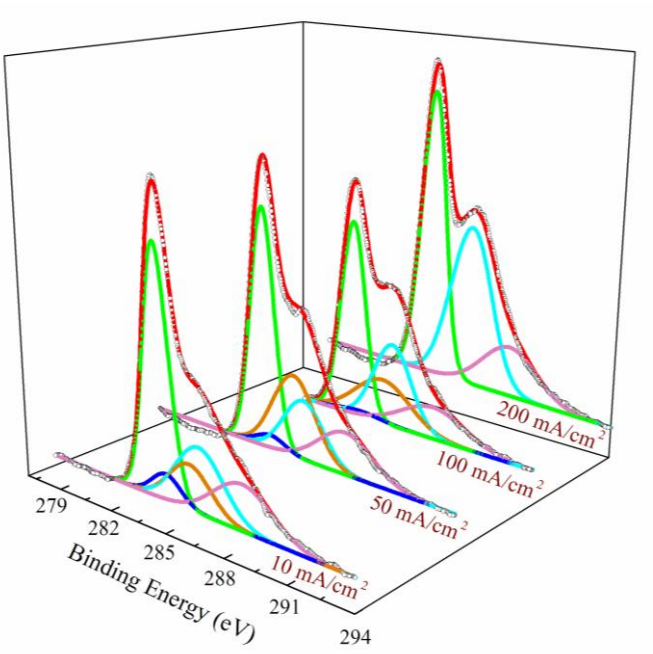

Figure 5. XPS C 1s curve fitting spectra of OGF versus the electro-oxidation current density.

As can be seen from Table 1, the larger the oxidation current density applied, the lower the content of defective carbon remains, indicating that the large oxidation current density tends to oxidize the defective carbon. Further more, the defective carbon atoms are easily oxidized to C=O or C-O-C at large oxidation current density. There might be different oxidation steps for samples at different oxidation current density. For the OGF oxidized at 10 mA/cm^2, a portion of defective carbon atoms are oxidized to C-OH by the active oxygen (O•) at first, and then the active oxygen (O•) tends to oxidize C-OH to C=O and COOH. For the OGF oxidized at 50 mA/cm^2, the first step is deeper than the OGF at 10 mA/cm^2, and more defective carbons are oxidized to C-OH. This suggests less choices for the subsequent oxidation reaction, since all the samples are oxidized to the same oxidation degree (560

mAh/g). The highest C-OH content of 24% can be obtained by using current density of 50 mA/cm^2. The C-OH content is lower and the C=O content is higher for the OGF oxidized at 100 mA/cm^2 compared with the OGF oxidized at 50 mA/cm^2. There is no C-OH exists for the OGF oxidized at 200 mA/cm^2, while the largest C=O content of 40% is obtained. The phenomenon may be explained as following. As the oxidation current density continually increases, a part of defective carbon might be not only oxidized to C-OH, but also directly oxidized to C=O or COOH, because more active oxygen (O•) is formed each time, which can provide a greater driving force for the oxidation reaction.

Table 1. The contents of various functional groups on the surface of GF and OGF.

Sample	Graphitized carbon 284.7 eV	Defective carbon 285.1 eV	C-OH 286.3 eV	C=O 286.8 eV	COOH 288.9 eV	Total content (–C-OH, –COOH)
GF [a)]	29%	34%	0	26%	11%	11%
OGF-10	44%	5%	13%	21%	17%	30%
OGF-50	41%	3%	24%	17%	15%	39%
OGF-100	39%	2%	19%	25%	15%	34%
OGF-200	44%	0	0	40%	16%	16%

a) Data obtained from our previous work [19].

In previous work, we have found that both C-OH and COOH surface functional groups can act as active sites to catalyze the oxidation reaction of VO^{2+} to VO_2^+ [19]. The proposed mechanism of OGF surface oxygen-containing groups toward VO^{2+}/VO_2^+ reaction is shown in Scheme 1. The change tendency of total content of C-OH and COOH (Table 1) on the surface of OGF agrees well with the oxidation peak current data (see Fig. 3), which confirms the reaction mechanism in Scheme 1.

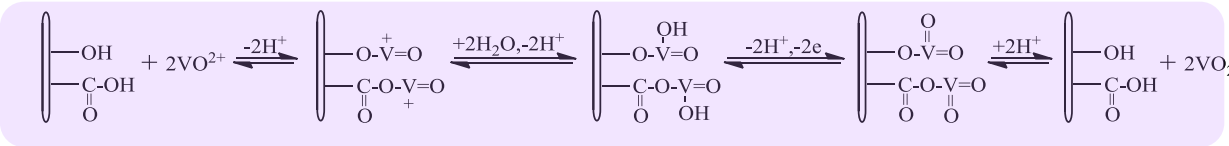

Scheme 1. The mechanism of OGF towards VO^{2+}/VO_2^+ redox reaction by surface –OH and -COOH groups.

3.3 VRB single cell performance

The charge–discharge test of the single VRB cell with GF and OGF as the electrode respectively was investigated at a current density of 40-80 mA/cm^2, and the charge–discharge curves are shown in Fig. 6 (a)-(e). It can be seen that the cells with OGF obtained at 10-100 mA/cm^2 present lower charging voltages and higher discharging voltages than that with pristine GF at all test current densities. This suggests the electro-oxidation treatment of GF reduces the polarization resistance

during the charge-discharge process, and as a result, the voltage efficiency is accordingly improved. On the contrary, the cell with OGF-200 presents a higher charging voltage and lower discharging voltage than the cell with pristine GF. This may be due to the excessive oxidation of the GF, which would decrease the electronic conductivity of the electrode network.

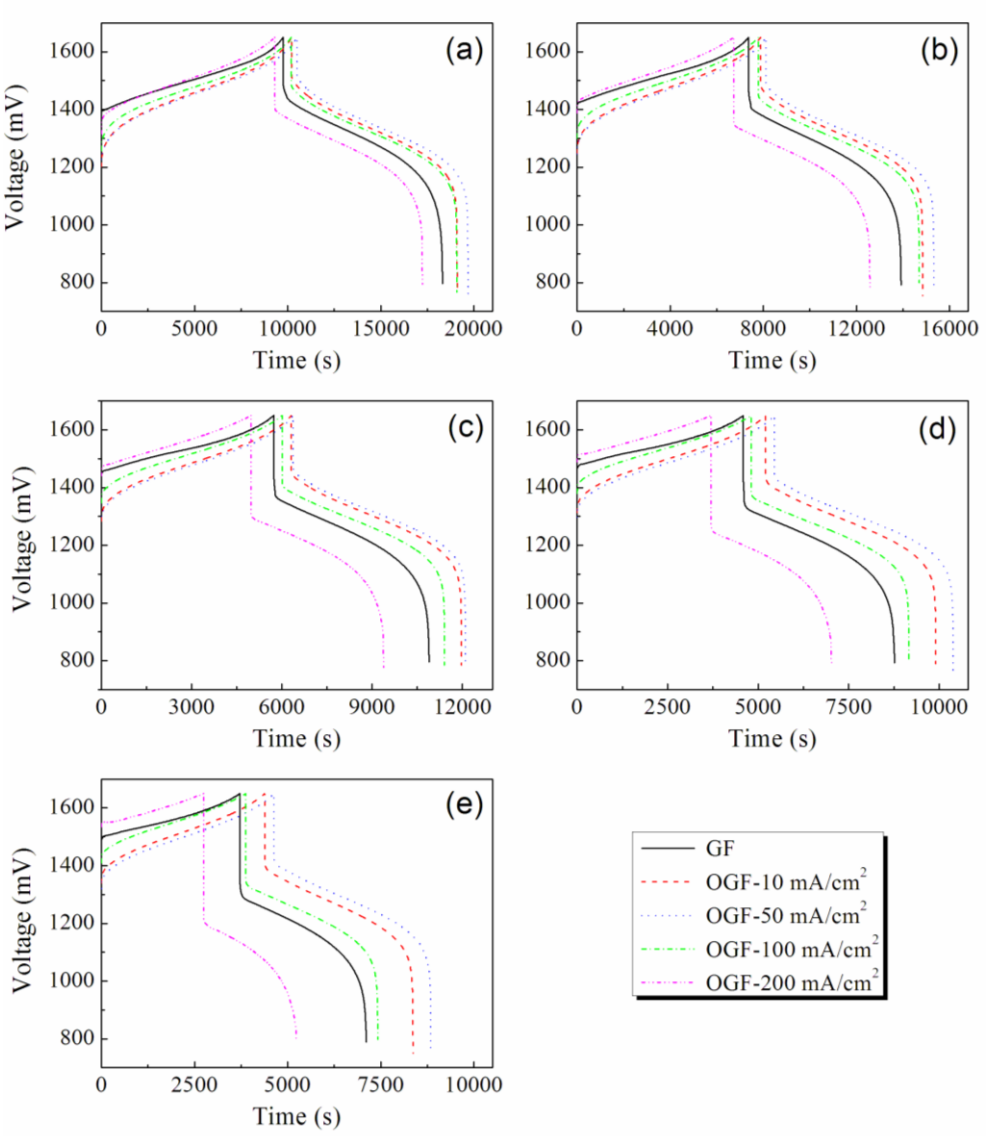

Figure 6. Charge-discharge curves of VRB single cell with GF and OGF as the electrode test at different current density. (a) 40 mA/cm^2, (b) 50 mA/cm^2, (c) 60 mA/cm^2, (d) 70 mA/cm^2, and (e) 80 mA/cm^2.

The voltage efficiency (VE) and energy efficiency (EE) of the single VRB cell at various current densities are shown in Fig. 7. As can be seen, both the VE and EE show the same change tendency with the electro-oxidation current density. The cell with OGF-50 exhibits the highest VE and EE at all testing current densities, agreeing well with the CV (Fig. 3) and EIS (Fig. 4) results.

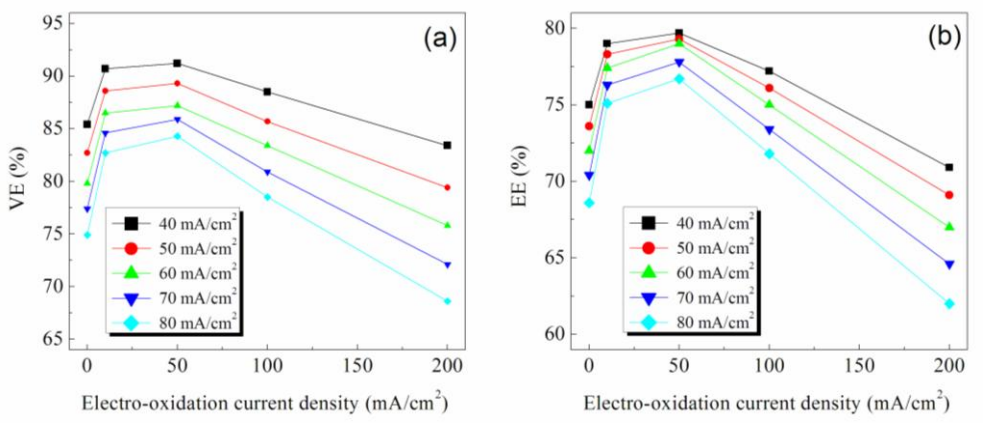

Figure 7. Voltage efficiency (VE) and energy efficiency (EE) of VRB single cell with GF and OGF as the electrode test at different charge-discharge current.

In order to understand the stability of the electrodes during charge-discharge test, the cycling performances of the VRB single cell using GF and OGF-50 as the electrode respectively were investigated at current density of 60 mA/cm^2 for 30 cycles and the corresponding cell efficiencies are illustrated in Fig. 9. As can be seen, both two cells show relative stable performances and the value of efficiency (VE and EE) changes very little with the number of cycles.

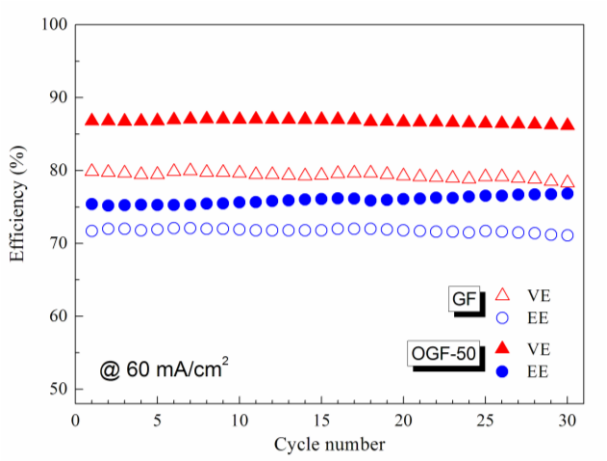

Figure 8. Cycle properties of VRB single cell with GF and OGF-50 as the electrode at 60 mA/cm^2.

The surface morphology and surface state of GF and OGF-50 were also studied before and after 30 cycles of charge-discharge test and the SEM images are shown in Fig. 9. Comparing Fig. 9 (a) and (b), it can be found that the surface morphology of pristine GF is very smooth and essentially unchanged after 30 cycles test. In the case of OGF-50, as shown in Fig. 9 (c) and (d), the surface morphology is rough and some surface etching flakes and dots can be seen, which were formed by electro-oxidation treatment. No significant change of element content and the proportion before and

after cell test are observed by the EDS analysis, suggesting that both GF and OGF-50 are very stable during cell charge-discharge test.

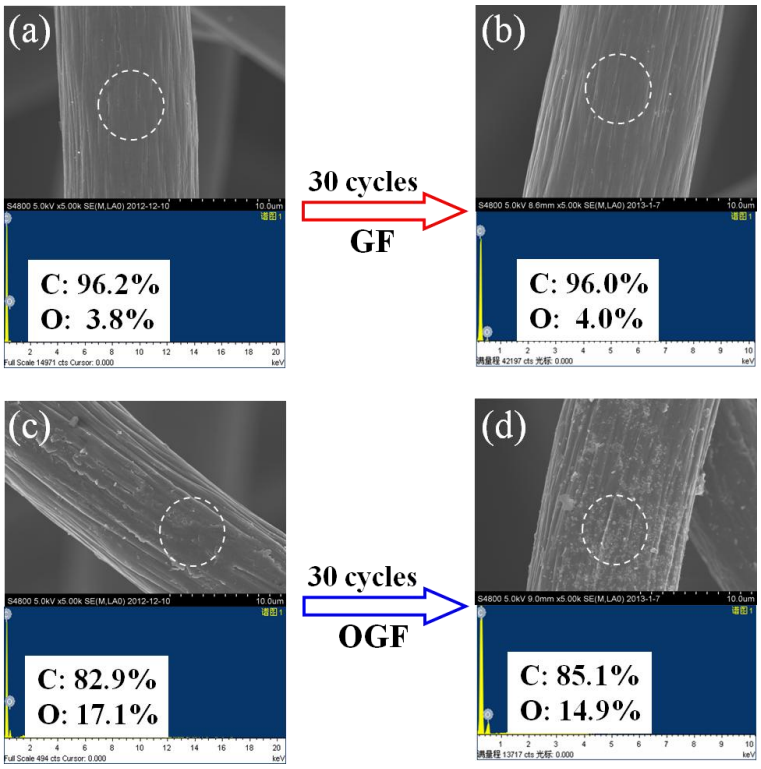

Figure 9. SEM images and EDS spectra of GF and OGF-50 electrode before and after VRB single cell test. (a) GF before test, (b) GF after test, (c) OGF-50 before test, and (d) OGF-50 after test.

4. CONCLUSIONS

An environmental friendly and controllable electro-oxidation technique is employed to improve the activity of graphite felt (GF) electrode for VRB application, by introducing numerous types of oxygen-containing surface functional groups and increasing the surface roughness. The effect of applied electro-oxidation current density on activity of oxidized graphite felt (OGF) is studied in details. The CV and EIS results show that the OGF obtained at 50 mA/cm^2 (OGF-50) has the highest oxidation current density and lowest charge transfer resistance towards VO^{2+}/VO_2^+ redox reaction, consistent with its largest content of C-OH and COOH surface active functional groups by XPS analysis. The VRB single cell with OGF-50 also exhibits the best cell performance, with an energy efficiency of 77% at 60 mA/cm^2.

ACKNOWLEDGEMENTS
This work was supported by the National Natural Science Foundation of China (20973099, 50606021), Shenzhen Science Fund for Distinguished Young Scholars (JC201104210149A) and the Science Foundation of Shenzhen (JCYJ20120830152316442, JC201005310703A, CXZZ20120614194136123, JC201005310712A).

References

1. B. Dunn, H. Kamath, J. M. Tarascon, *Science*, 334 (2011) 928.
2. Z. G. Yang, J. Zhang, M. C. W. Kintner-Meyer, X. Lu, D. Choi, J. P. Lemmon, J. Liu, *Chem. Rev.*, 111 (2011) 3577.
3. M. Skyllas-Kazacos, M. H. Chakrabarti, S. A. Hajimolana, F. S. Mjalli, M. Saleem, *J. Electrochem. Soc.*, 158 (2011) R55.
4. P. Leung, X. Li, C. Leon, L. Berlouis, C. T. J. Low, F. C. Walsh, *RSC Adv.*, 2 (2012) 10125.
5. K.L. Huang, X.G. Li, S.Q. Liu, N. Tan, L.Q. Chen, *Renewable Energy*, 33 (2008) 186.
6. L. Liu, J. Xi, Z. Wu, W. Zhang, H. Zhou, W. Li, X. Qiu, *J. Appl. Electrochem.*, 42 (2012) 1025.
7. S. Peng, N. Wang, C. Gao, Y. Lei, X. Liang, S. Q. Liu, Y. Liu, *Int. J. Electrochem. Sci.*, 7 (2012) 4388.
8. S. Li, K. Huang, S. Q. Liu, D. Fang, X. Wu, D. Lu, T. Wu, *Electrochim. Acta*, 56 (2011) 5483.
9. J. Xi, Z. Wu, X. Qiu, L. Chen. *J. Power Sources*, 166 (2007) 531.
10. X. Teng, Y. Zhao, J. Xi, Z. Wu, X. Qiu, L. Chen, *J. Power Sources* 189 (2009) 1240.
11. J. Xi, Z. Wu, X. Teng, Y. Zhao, L. Chen, X. Qiu. *J. Mater. Chem.*, 18 (2008) 1232.
12. B. Sun, M. Skyllas-Kazacos, *Electrochim. Acta*, 37 (1992) 1253.
13. B. Sun, M. Skyllas-Kazacos, *Electrochim. Acta*, 37 (1992) 2459.
14. C. Gao, N. Wang, S. Peng, S. Q. Liu, Y. Lei, X. Liang, S. Zeng, H. Zi, *Electrochim. Acta*, 88 (2013) 193.
15. B. Sun, M. Skyllas-Kazakos, *Electrochim. Acta*,.36 (1991) 513.
16. W. Wang, X. D. Wang, *Electrochim. Acta*, 52 (2007) 6755.
17. F. He, *Carbon Fiber and Graphite Fiber*, Chemical Industry Press, Beijing (2010).
18. X. Li, K. Huang, S. Liu, N. Tan, L. Chen, *Trans. Nonferrous Metals Soc. China*, 17 (2007) 195.
19. W. Zhang, J. Xi, Z. Li, H. Zhou, L. Liu, Z. Wu, X. Qiu, *Electrochim. Acta*, 89 (2013) 429.
20. L. Yue, W. Li, F. Sun, L. Zhao, L. Xing, *Carbon*, 48 (2010) 3079.
21. C. Yao, H. Zhang, T. Liu, X. Li, Z. Liu, *J. Power Sources*, 218 (2012) 455.
22. J. Xi, X. Ma, M. Cui, X. Huang, Z. Zheng, X. Tang, *Chinese Sci. Bull.*, 49 (2004) 785.